JOINT EUROPEAN TORUS

JET–P(89)18

A. Boileau, M. von Hellermann, L.D. Horton, H.P. Summers,
P.D. Morgan and JET Team

Low-Z Imputity Behaviour in JET from Charge-Exchange Spectroscopy Measurements

Low-Z Imputity Behaviour in JET from Charge-Exchange Spectroscopy Measurements

A. Boileau[1], M. von Hellermann, L.D. Horton[2], H.P. Summers, P.D. Morgan and JET Team*

JET-Joint Undertaking, Culham Science Centre, OX14 3DB, Abingdon, UK

[1]Centre Canadien de Fusion Magnetique, 1804 Montee Ste-Julie, Varennes, Canada, JOL 2PO.
[2]ORNL, P.O. Box Y, Oak Ridge, TN, 37831, U.S.A.
** See Appendix 1*

Preprint of Paper to be submitted for publication in
Nuclear Fusion

LOW-Z IMPURITY BEHAVIOUR IN JET FROM CHARGE EXCHANGE SPECTROSCOPY MEASUREMENTS

A Boileau*, M von Hellermann, L D Horton**,
H P Summers and P D Morgan

JET Joint Undertaking, Abingdon, Oxon OX14 3EA, UK

Present address: * Centre Canadien de Fusion Magnétique,
1804 Montée Ste-Julie, Varennes,
Canada JOL 2PO

** ORNL, PO Box Y, Oak Ridge, TN, 37831, USA

ABSTRACT

Absolute densities of the dominant light impurities in the plasma centre are measured during neutral beam heating using charge exchange spectroscopy. The behaviour of carbon, oxygen and helium (in helium discharges) is investigated for limiter and X-point discharges. When the plasma is in the X-point configuration, the central carbon concentration is significantly lower than in the material limiter configuration. After the transition from L to H-mode, a strong impurity build up is observed in the plasma centre which significantly reduces the central dilution factor n_D/n_e from initial values near 0.8 to about 0.6 at the collapse of the H-mode. Nonetheless, during the H-mode, the product of deuteron density and ion temperature $n_D T_i$ (both derived by the charge exchange spectroscopy diagnostic) shows a clear enhancement with respect to the L-mode at the same input power. Helium discharges, as compared to deuterium discharges, have a higher carbon concentration (consistent with physical sputtering) and a much reduced oxygen concentration ($n_O/n_e < 0.005$; consistent with chemical release of oxygen). The transient behaviour of oxygen and carbon following deuterium pellet injection is discussed using a comparable non-pellet reference discharge. An increase of the oxygen content in the plasma centre is observed some 600 msec after injection of a deuterium pellet, while the central carbon density appears only transiently diluted by the sudden addition of pure deuterium. No evidence of a cleaning action through sawtooth relaxations is detected in the case of low-Z impurities.

1. INTRODUCTION

The study of low-Z impurities is particularly important during neutral beam (NB) heating on JET since NB injection is routinely used to trigger the transition to H-mode and, together with other means of heating and fuelling, has produced the best performances so far obtained on JET [1]. The presence of carbon and oxygen, the dominant impurities, greatly affects the dilution of fusion fuel in the plasma centre and plays a role in the energy balance at the edge via radiation losses.

During NB injection, low-Z ions are fully stripped over most of the plasma minor radius because of the high temperatures attained. Line emission from partly ionised atoms is thus limited to the periphery and may be used only indirectly, and with low reliability, to deduce the absolute impurity density in the centre. Over most of the plasma, low-Z impurity-induced radiation is essentially restricted to bremsstrahlung. The line integrated bremsstrahlung level is, however, not a measure of the local impurity content and reconstruction of the Z_{eff} profile using a multichord system remains difficult [2]. Furthermore, bremsstrahlung measurements do not resolve the contributions from different impurities.

Fully stripped ions may, however, be studied using charge exchange spectroscopy (CXS) [3,4]. The diagnostic is based on the charge transfer reaction between the impurity nucleus A^Z and the fast neutral D:

$$A^Z + D \rightarrow (A^{Z-1})^* + D^+ \qquad (1)$$

The JET heating beams provide a source of energetic deuterium atoms. The 'recoil' hydrogen-like impurity ion is left in an excited state and radiates at specific wavelengths as it is de-excited to lower quantum states. Several of these transitions lie in the visible and their spectral characteristics have been used to measure the ion temperature [5,6] and toroidal rotation velocity on JET [5,7]. More recently, the capabilities of the CXS diagnostic were extended to include local magnetic field and Z_{eff} measurements using motional Stark features in the Balmer spectrum of deuterium [8]. The observed intensity may also be used to derive an absolute impurity density [5,9-12]. This is a complex process which involves, in particular, the modelling of NB attenuation to obtain the fast neutral density.

We have sought to identify and quantify the sources of uncertainty inherent in the calculation of absolute impurity densities using visible transitions. According to this analysis, the absolute values quoted in this paper are not known to better than ± 40%. The effective ion charge (Z_{eff}) reconstructed from simultaneous measurements of carbon and oxygen shows satisfactory agreement with average values inferred from the bremsstrahlung level, within the error bars of both diagnostics. On the other hand, since most of the uncertainty comes from the primary capture rate coefficient, which does not depend sensitively on plasma parameters, the evolution of the calculated impurity density is more reliable (≤ 15%). Charge exchange spectroscopy can greatly improve our knowledge of low-Z impurity behaviour in the plasma centre during NB injection and so is a new and major contributor to this continuing effort on JET [13-19].

2. EXPERIMENTAL SETUP AND METHODOLOGY

The charge exchange diagnostic results reported in this paper are based on a single vertical line of sight that intercepts all neutral beams in the plasma centre. (A multichord CXS system has recently been installed on JET. Impurity radial profile results from this will be reported in a later work.) This cross beam technique provides good spatial resolution, defining an observation volume with dimensions typically 5% of the plasma minor radius.

The fast injected deuterium atoms have a full energy of 40 keV/amu. The available power of 10 MW is distributed into full, half and third energy components, corresponding to the acceleration of D^+, D_2^+ and D_3^+, in proportions of 0.76:0.17:0.07 [20].

The light is collected by a lens system and transmitted by optical fibres to remote spectrometers and detectors (Fig.1). Fibre transmission characteristics limit the accessible spectral range to the visible part of the spectrum. The light is divided at the spectrometer end using a beam splitter so as to monitor two transitions of different impurities simultaneously. Each spectrometer is equipped with an intensified linear array with a full spectrum recorded approximately every 20 ms, depending on signal strength. The whole detection arrangement is absolutely calibrated using a tungsten lamp. The composite spectrum is typically made up of 300 to 600 points and is dominated by the charge exchange feature. Additional lines are observed on some spectra but all components are unambiguously resolved using a multi-Gaussian fit. A more detailed description of the experimental setup and observed transitions can be found in ref.[5].

The measured intensity $I(n - n')$ is related to the impurity density $n(A^Z)$ according to:

$$I(n - n') = q(n - n') \int_{o.v.} n(D)\, n(A^Z)\, dv \qquad (2)$$

The integral is performed over the observation volume and depends sensitively on the geometry. The fast neutral density $n(D)$ is obtained from an attenuation code that uses the experimental electron density and temperature profiles from the JET database. For plasma conditions studied in this paper, impurity stopping may account for up to 20% of the attenuation and is taken

into account using the effective charge given by the bremsstrahlung level, assuming a carbon to oxygen ratio of 3. Departures from these typical conditions are found to have little impact on the result. Simulations have also shown that the attenuation factor computed near r=0 is insensitive to the radial electron profile. This is because, in the present central plasma observations, the attenuation depends on the line integral density (accurate to within 1% independent of the profile shape), and because the attenuation cross-sections are only a weak function of the electron temperature.

The calculation of the effective charge exchange rate coefficient $q(n - n')$ in eq.2 is based on the Unitarized-Distorted-Wave-Approximation (UDWA) model [21,22]. It is corrected for cascading from upper n" levels ($n" < 20$) and collisional redistribution among the ℓ states [23]. The consistency of the atomic database was checked by observing several transitions of the same element by splitting the light of one viewing line into two spectrometers, thus simultaneously recording the CX spectra from the same observation volume. Deviations from expected values for visible transitions are of order 30%. A better estimate of the uncertainty attached to rate coefficients would require simultaneous measurement of UV and visible lines.

3. EXPERIMENTAL RESULTS

3.1 Effective ion charge

From simultaneous measurements of the two dominant impurities in the plasma, the effective ion charge can be calculated as:

$$Z_{eff} = 1 + \sum_i Z_i(Z_i-1) \frac{n_{Z_i}}{n_e} \qquad (3)$$

For standard operating conditions of JET, carbon and oxygen are by two orders of magnitude the most important impurities and are largely responsible for the difference of Z_{eff} from unity. Heavy impurity concentrations, especially nickel, rarely reach 0.01% and do not make significant contributions to Z_{eff} under normal operating conditions. In cases where helium is used as filling gas, the oxygen concentration is typically low, < 0.5%, and has little influence on the effective ion charge or the dilution factor. Helium and carbon are then observed simultaneously.

The effective ion charge reconstructed from CXS measurements is compared in Fig.2 to the value deduced from the visible bremsstrahlung level. The two sets of measurements agree within the experimental error bars. It is to be noted that charge exchange measurements are localised in the plasma centre while the bremsstrahlung level gives a chord average estimate of Z_{eff}, weighted by the electron density squared and a weakish function of electron temperature. Differences between the two diagnostics may therefore appear if the ion effective charge profile is not flat. We find no systematic deviation between the two diagnostics over the density range investigated $n_e \sim 1\text{-}7\times10^{19}$ m^{-3}. This strongly supports the analysis procedure since the bremsstrahlung photon flux increases as n_e^2, while the CXS raw signal decreases exponentially with n_e because of beam attenuation. The Z_{eff} measurements also show broad agreement with the deuterium content inferred from fusion reaction rate measurements [24].

The comparison shown in figure 2 confirms the reliability of the charge exchange data. The strength of the diagnostic, however, is that it can

resolve the contribution of each low-Z impurity. This is critical, since for example, the same effective ion charge has been obtained with a carbon to oxygen ratio of C/O∿1.5-2.0 in 2 MA X-point plasmas and C/O∿10 in 5 MA limiter plasma (Z_{eff} = 2.8 in both cases). As mentioned in the introduction, the absolute error bar on charge exchange measurements of impurity densities is substantial and so most of the results presented in the following sections will emphasize the time evolution of the impurity concentration or the comparison of different operating conditions of JET.

3.2 Magnetic configuration

JET may be operated with a number of different magnetic configurations which affect particle confinement, plasma-wall interaction and recycling. We contrast JET operation with a material limiter (carbon limiters or carbon protection tiles covering the inner wall; I_p < 6 MA) to operation with a magnetic limiter (X-point with a single-null magnetic separatrix near the top of the vessel; I_p < 4.5 MA) [25].

Figure 3a shows carbon and oxygen densities observed with a material limiter (JET pulse 10711, I_p = 2 MA). The evolution of the electron density on axis and the total beam power are displayed in Fig.3b. Carbon is more abundant than oxygen although the ratio C/O decreases during NB injection with this magnetic field configuration. As will be shown in a later section, the oxygen density tends to follow the deuterium density, which increases during injection. The subsequent JET pulse was produced with the same plasma current but with an X-point magnetic limiter (Fig.3b). Figure 4b shows the electron density on axis, Hα and the total beam power. For these consecutive pulses it is expected that wall conditions should be almost identical. In the X-point magnetic configuration an H-mode can be achieved whereupon the particle and energy confinement are significantly better than in the normal mode (L-mode).

Comparing Figs.3a and 4b, it is seen that during the L-mode phase, the oxygen density is close to that for the material limiter case, when the macroscopic plasma parameters such as electron density and plasma current are similar. The apparent agreement between the two oxygen

density traces thus suggest similar screening and confinement by the two magnetic field configurations. Also, the geometry of the last closed flux surface is likely to have little impact on the oxygen content since most of the oxygen actually originates from the wall rather than from the surface directly in contact with the plasma [15]. On the other hand, the carbon density is reduced by a factor of 2 to 3 in the magnetic limiter case. This could be explained by a better screening of incoming carbon ions by particle outflow in the X-point region [16]. We also note that the carbon to oxygen ratio usually increases during NB injection with magnetic limiter, irrespective of the transition from L to H-mode.

The H-mode phase is characterized by a sudden drop in the recycling and a steep increase of the electron density as shown respectively by the Hα and the electron density traces in Fig.4b. It is an attractive regime since the energy confinement, τ_E, increases by a factor of 2 to 3. However, Fig.5 clearly indicates that the low-Z impurity densities in the plasma centre increase faster than the deuterium density, resulting in an impurity build up. For all cases where carbon and oxygen were monitored simultaneously, the impurity concentrations started to increase at the transition to the H-mode. This severely affects the deuterium dilution (calculated by subtracting the impurity contribution from the electron density) (Fig.5). During the L-mode phase, the deuterium concentration increases slightly because of beam fuelling. The higher impurity concentrations during the H-mode phase gradually dilute the fusion fuel. This is a significant concern long before impurity radiation losses threaten the stability of the discharge. Based on these results, the steep increase of the electron density in the plasma centre is inferred to be largely due to the retention of low-Z impurities. Tests show that the observation of a low-Z impurity increase is not an artifact of the beam attenuation calculation. However, the observation cannot be unambiguously attributed to impurity accumulation since the impurity concentration profile evolution is not known from the CXS diagnostic.

Machine performance with different magnetic field configurations can be assessed by combining the ion temperature and the deuterium density, both deduced from CXS spectroscopy measurements. With a material

limiter, the product $n_D T_i$ increases linearly with the total input power to the plasma (Fig.6a). High power results also correspond to high plasma currents. For the X-point configuration the L-mode phase follows the dependence shown in fig.5a for a material limiter. In the H-mode phase, however, the product $n_D T_i$ reaches significantly higher values for the same input power (Fig.6b). The line shown in Fig.5b reproduces the dependence observed for a material limiter. At the transition to H-mode, central plasma parameters still correspond essentially to the L-mode, which explains why several points fall on the line. In some cases, the impurity buildup is such that the product $n_D T_i$ saturates before the end of the H-mode.

3.3 Helium plasmas

Helium is often used as minority species during radio-frequency heating experiments. Under these conditions, the helium charge exchange signal is usually too small to be unambiguously isolated from the composite spectrum. Helium may however be observed when it is used as prefill gas.

The impurity content of helium plasmas was investigated by observing low-Z elements in pairs using the beam splitter arrangement. For the magnetic limiter case, the carbon concentration is typically 6% and increases during injection, oxygen is 0.5% or less and helium is close to 30% of the electron density (Fig.7a). The evolution of the electron density on axis and the total beam power are shown in Fig.7b. The low oxygen concentration is associated with a low deuterium content which is estimated to remain below 20% even during injection. This is interpreted as evidence that oxygen release from the wall is by chemical reactions. The higher carbon concentration, compared with deuterium plasmas, may be due to the higher sputtering yield of helium compared to deuterium (physical sputtering). This is based on the interpretation of impurity influxes indicating that the carbon sputtering yield is about twice as large in the case of helium as for deuterium for $n_e \gtrsim 2 \times 10^{19}$ m^{-3} [27]. As for deuterium plasmas, the present results show that the carbon concentration in helium discharges is higher with a material limiter than with a magnetic limiter (Fig.8a). The corresponding electron density on axis and total beam power traces are displayed

in Fig.8b. At the beginning of injection the sum of electrons contributed by carbon and helium adds up to the measured electron density.

3.4 Pellet injection

High velocity deuterium pellets are injected in the plasma to increase the density. To study the effect of pellet injection on low-Z impurity concentrations, two JET pulses with and without pellets which had similar electron densities at times just before and long after the pellet are considered (Fig.9). In both cases, NB injection starts at 12s and, for one of these pulses, this coincides with the injection of a deuterium pellet. In the reference case, the electron density slowly increases due to neutral beam fuelling. Pellet injection drastically changes the shape of the density profile, which complicates the beam attenuation calculation. However, the density profile relaxes rapidly (compared to our sampling rate) towards a profile peaked on axis. As noted in section 2, the beam attenuation calculation near $r = 0$ is more sensitive to the line integral density than to the profile shape. The effect of the changing plasma environment on collisional redistribution among the ℓ states is also taken into account when computing the effective charge exchange rate coefficient [5].

Figure 10 shows the evolution of the carbon concentration in the plasma centre for the two pulses. The charge exchange signal is observed only after the start of NB injection so that the effect of the pellet can already be seen on the first spectra. The pellet plasma is characterized by a strong reduction of the carbon concentration with respect to the reference case. However, the carbon densities evaluated near 12.3s for both are within 10% of each other. It is concluded that the lower carbon concentration simply results primarily from the diluting effect of the massive pure deuterium injection in the pellet case. After the pellet transient, no significant difference is observed in the carbon concentration (or density).

The situation is markedly different for oxygen. The carbon to oxygen ratio for the same two pulses is reproduced in Fig.11. The present method has an advantage in considering the ratio of impurity concentra-

tions measured simultaneously using the same line of sight since the result no longer depends on uncertainties related to geometry or beam attenuation calculation. If the behaviour of oxygen were the same as for carbon, the C/O ratio would be the same for both pulses. On the contrary, a strong dip of the carbon to oxygen ratio (possibly delayed some 0.6s after the pellet is injected) is observed. A plausible explanation is a net release of oxygen following the pellet injection and probably due to the increased deuterium flux to the wall following pellet ablation in the plasma periphery. As evidenced by the results in helium discharges, deuterium releases oxygen by molecule formation which quickly desorbs from the wall (wall temperature $\simeq$ 300°C). The oxygen flux from the wall was unfortunately not available for these pulses but the observation that the higher oxygen content in the plasma centre appears slightly delayed with respect to the maximum on the electron density trace is reasonable.

3.5 Sawtooth relaxations

Observation of impurity line emission during sawteeth in TFR has led to the conclusion that these relaxations expel impurities selectively compared with electrons [28]. In that work, most of the impurity line emission modulation was actually attributed to changes in the electron temperature. After correcting the signal accordingly, the residual part of the modulation was interpreted as a cleaning action of the sawteeth. The same approach was used on Alcator, leading however to the opposite conclusion [29]. In the latter case, all the intensity modulation was attributed to electron temperature relaxations.

Although the absolute impurity concentration deduced from charge exchange spectroscopy measurements has a large uncertainty, it can still be used for detecting variations as a function of time correlated with sawtooth relaxations. It is essential to ensure that the NB power does not change as a function of time, since it is difficult to account accurately for such variation in the signal intensity. Figure 12 shows the ion temperature and line intensity from a carbon transition, with injected NB power strictly constant at 4 MW. Large sawtooth relaxations of order 25% are apparent on the ion temperature. The light intensity

remains however approximately constant. The carbon concentration in the plasma centre estimated from this signal leads to the same conclusion as it also remains approximately unchanged during the sawtooth relaxations. According to these results, the impurity density in the plasma centre behaves similarly to the electron density and corroborates the Alcator results (which were obtained in a very different way).

CONCLUSIONS

Visible spectral emission following charge exchange from neutral deuterium in the JET heating neutral beams has been used to deduce light impurity densities, and indirectly deuterium densities, in the plasma core. The time evolution of these densities has been explored by this method for different magnetic field configurations (limiter and X-point) and during sawteeth and pellet injection. The higher carbon concentration in helium than in deuterium plasmas shows that physical sputtering is largely responsible for the carbon production, helium having a higher sputtering yield than deuterium. There is also some evidence that the carbon to oxygen ratio increases with total input power, as expected, if carbon is released by physical sputtering whereas oxygen is not. The carbon content in the plasma centre is affected by the geometry of the magnetic flux surfaces near the plasma edge. The central carbon concentration is lower in the X-point L-mode case than in the limiter case. The transition to H-mode is, however, characterised by a strong increase of both carbon and oxygen concentrations leading to a decrease in the dilution factor.

Fully stripped oxygen in the plasma centre is related to the deuterium flux to the wall and carbon protecting tiles, indicating that chemical sputtering is largely responsible for oxygen production. This is supported by the evidence of a significantly reduced oxygen concentration in helium plasmas and deuterium plasmas following helium cleaning discharges. The link between oxygen and helium is also apparent during pellet injection, where a higher deuterium flux to the wall following pellet ablation is invoked to explain the transient enhancement of oxygen concentration some 0.6 sec after pellet injection.

The results show the unique capability of the charge exchange diagnostic to provide spatially and temporally resolved measurements of the dominant

impurities. Comparison of Z_{eff} values derived from oxygen and carbon concentrations shows reasonable agreement with averaged values of Z_{eff} derived from visible bremsstrahlung. However, the fact that distinctly different shapes of radial profiles of the electron density are observed for example in pellet fuelled plasmas or H-mode operation indicate the need for a further refined analysis of impurity accumulation and the measurement of complete radial profiles.

ACKNOWLEDGEMENT

The authors are greatly indebted to members of the JET team for operating the tokamak and, in particular, to the diagnosticians who have made their data available to us. We also thank Drs W Engelhardt and K Behringer who have stimulated this work as part of the JET impurity diagnostic programme. Helpful comments by Drs G McCracken, S Pitcher and P Harbour on plasma wall interactions are acknowledged.

REFERENCES

[1] JET report JET-P(88)15, 1988 - many authors.

[2] P D Morgan and J J O'Rourke, 14th EPS Meeting, Madrid, Spain (1987), JET-P(87)23.

[3] R C Isler, Phys.Rev.Lett. 38(1987)1359.

[4] R J Fonck, D S Darrow, K P Jaehnig, Phys.Rev A 29 (1984)3288.

[5] A Boileau, M von Hellermann, L D Horton, J Spence, and H P Summers, Plasma Physics and Cont. Fusion (1989) accepted for publication.

[6] S Corti, A Boileau, G Bracco, M Forrest, M von Hellermann, L Horton, P Larsen, C Sack, H P Summers, A Taroni, and F Tibone, 15th EPS Meeting, Dubrovnik, Yugoslavia, 1988.

[7] N C Hawkes, M von Hellermann, A Boileau, L Horton, E Källne, N J Peacock, J Ramette, and D Stork, 15th EPS Meeting, Dubrovnik, Yugoslavia, 1988.

[8] A Boileau, M von Hellermann, W Mandl, H P Summers, H Weisen, A Zinoviev, J.Phys.B (1989) accepted for publication.

[9] A N Zinoviev, A A Korotko, E R Krzhizhanovskij, V V Afrosimov, and Yu-S Gordeev, JEPT Lett 32(1980)539.

[10] R C Isler, L E Murray, S Kasai, J L Dunlap, S C Bates, P H Edmonds, E A Lazarus, C H Ma, and M Murakami, Phys.Rev. A 24(1981)2701.

[11] R J Fonck, M Finkenthal, R J Goldston, D L Herndon, R A Hulse, R Kaita, and D D Meyerhofer, Phys.Rev.Lett 49(1982)737.

[12] TRF Group, Phys.Lett. 122A(1985)29.

[13] W W Engelhardt, Plasma Physics & Controlled Fusion 28(1986)1401.

[14] M F Stamp et al., J. Nucl. Mater. 145(1987)236.

[15] K H Behringer, J. Nucl. Mater. 145(1987)145.

[16] K H Behringer et at., 11th IAEA Conf. on Plasma Physics & Controlled Fusion Research, Kyoto, Japan, p.197 (1986).

[17] B Denne et al., 14th European Conf. on Controlled Fusion & Plasma Physics, Madrid, Spain, p.109 (1987).

[18] K H Behringer, 15th European Conf. on Controlled Fusion & Plasma Physics, Dubrovnik, Yugoslavia, p.??? (1988).

[19] M F Stamp et al., 8th Int. Conf. on Plasma Surface Interactions in Controlled Fusion Devices, Julich, Germany (1988).

[20] G Duesing and the JET Team, Plasma Phys.Cont.Fusion, 28(1986)1429.

[21] H Ryufuku and T Watanabe, Phys.Rev. A 18(1978)2005.

[22] H Ryufuku, Phys.Rev. A 25(1982)720.

[23] J Spence and H P Summers, J.Phys. B 19(1986)3749.

[24] O N Jarvis, J M Adams, S Conway, J G Cordey, et al., 16th European Conf. on Cont. Fusion and jPlasma Physics, Venice, Italy (1989).

[25] A Tanga, K H Behringer, A E Costley, M Brusati, B Denne et al., Nuclear Fusion 27(1987)1877.

[26] M Keilhacker, K Lackner, J.Nucl.Mater. 111/112(1982)370.

[27] M F Stamp, M J Forrest, P D Morgan, H P Summers, 16th European Conf. on Controlled Fusion and Plasma Physics, Venice, Italy (1989).

[28] TFR Group, Nuclear Fusion, 25(1985)981.

[29] J Castracane, W L Hodge, and H W Moos, J.Quant.Spectrosc.Radiat. Transfer, 29(1983)157.

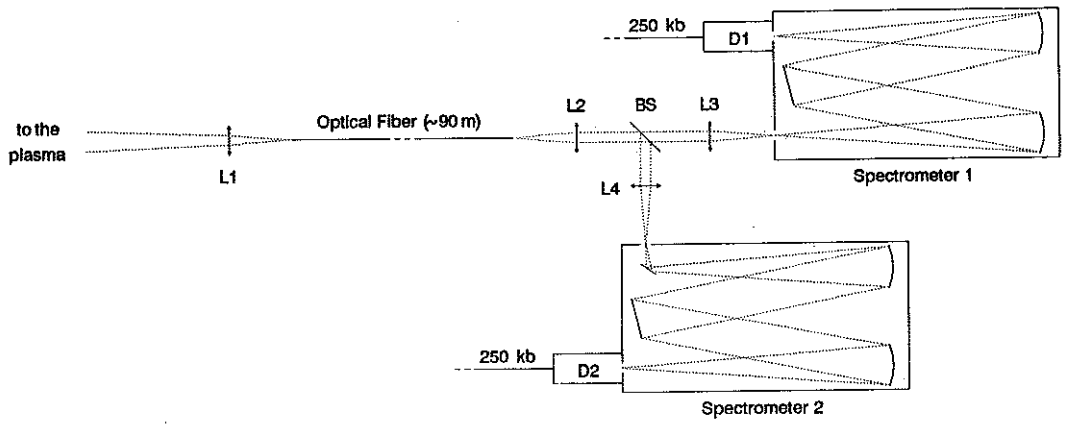

Fig. 1 Schematic view of the optical system. The beam splitter is used to divide the light into two spectrometers and observe two impurity lines simultaneously.

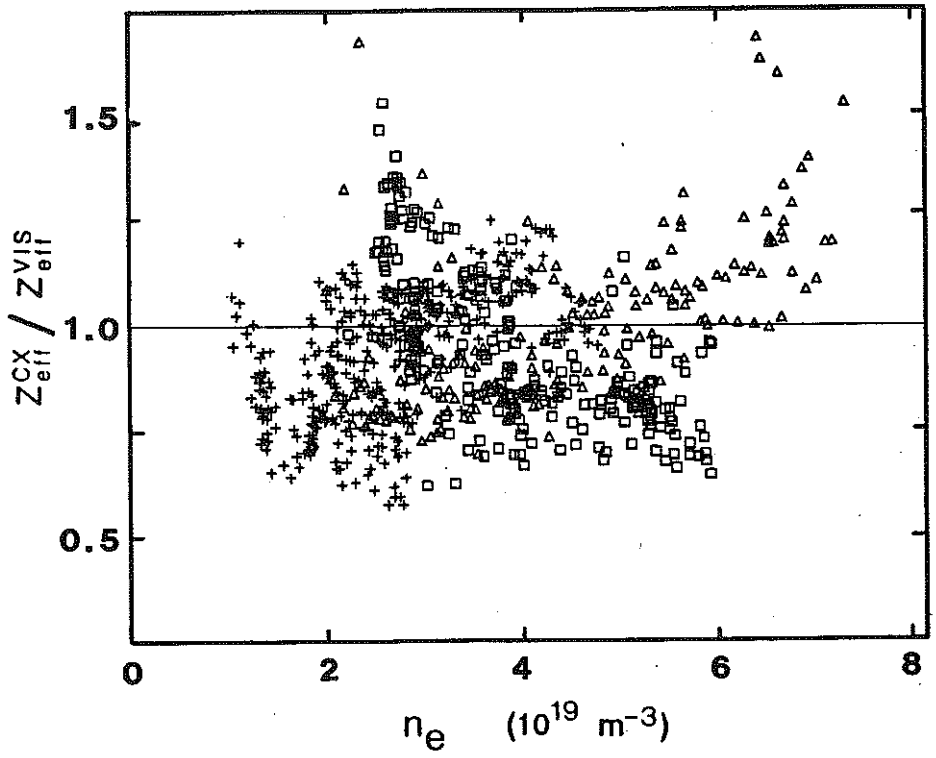

Fig. 2 Comparison between Z_{eff} obtained from charge exchange measurements (CX) and from visible Bremsstrahlung (VIS). Different transitions were used to obtain Z_{eff}: carbon n = 8-7 and oxygen n = 9-8 (circles), carbon n = 8-7 and oxygen n = 10-9 (triangles), carbon n = 8-7 and helium n = 4-3 for helium discharges (squares). The values of Z_{eff} range between 2.5 and 4.5 in limiter and X-point discharges.

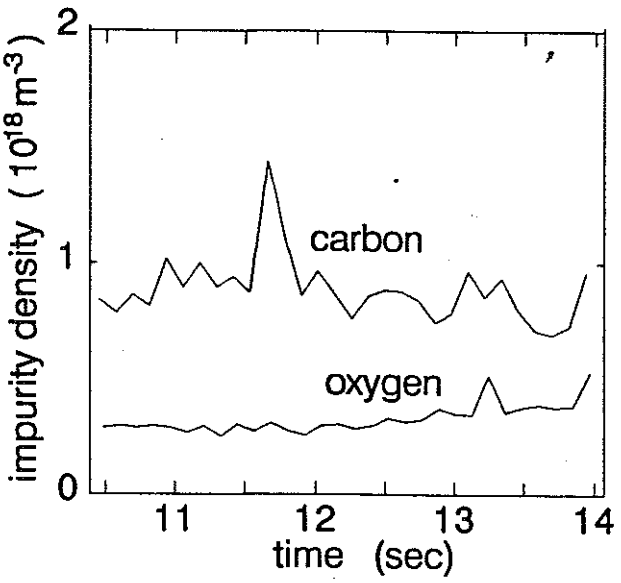

Fig. 3a Evolution of the central carbon and oxygen densities with a material limiter (JET pulse 10711, $I_p = 2$MA).

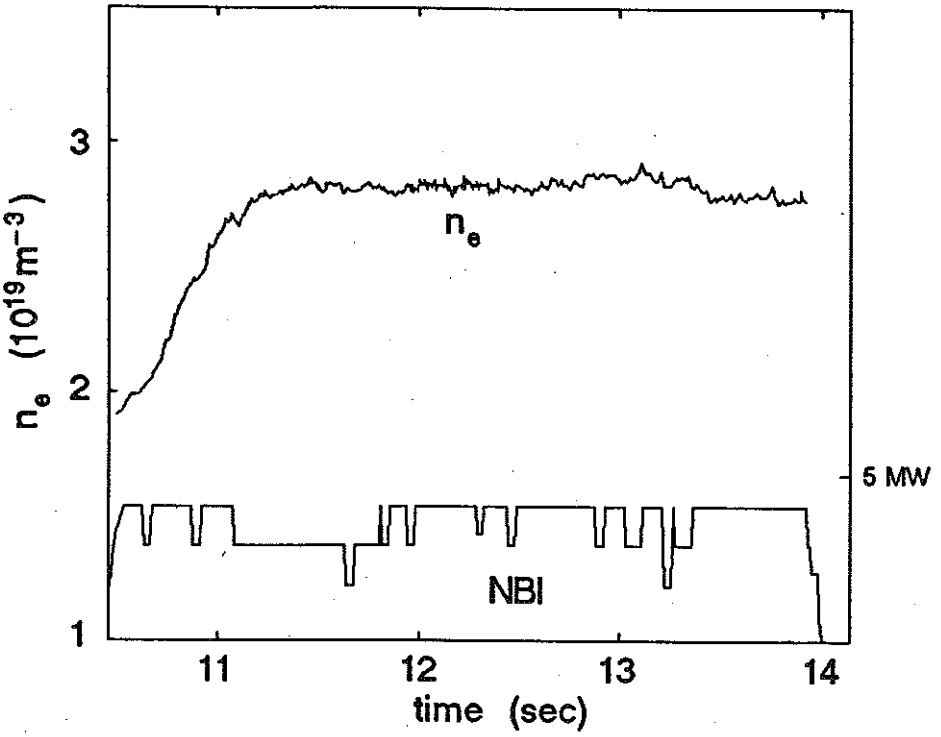

Fig. 3b Evolution of the electron density on axis and the total beam power during pulse 10711.

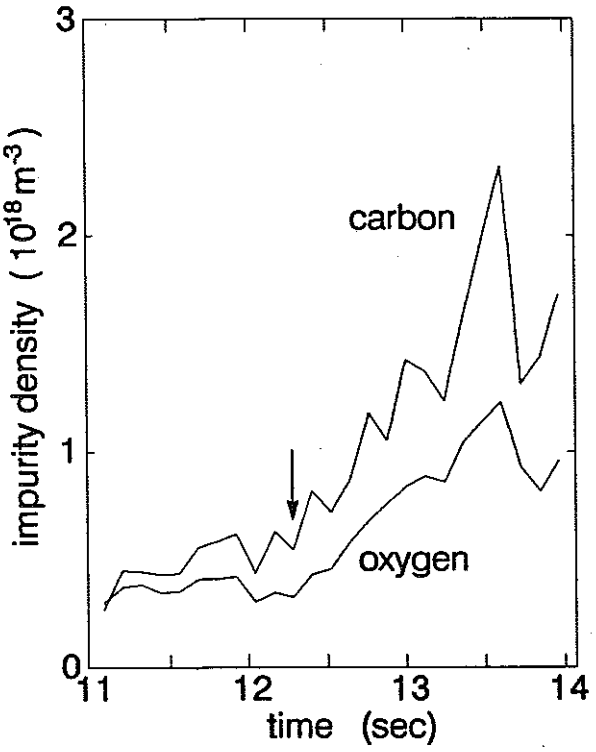

Fig. 4a Evolution of the central carbon and oxygen densities with a magnetic limiter (JET pulse 10713, $I_p = 2$MA). The arrow indicates the L to H-mode transition as deduced from the Hα trace.

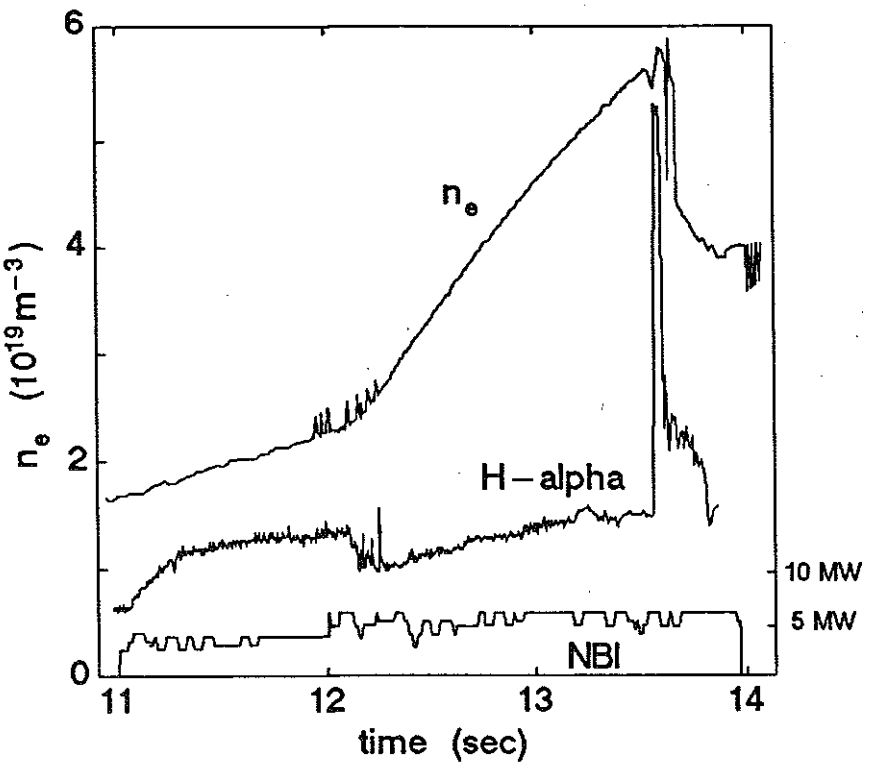

Fig. 4b Evolution of the electron density on axis, Hα and the total beam power during pulse 10713.

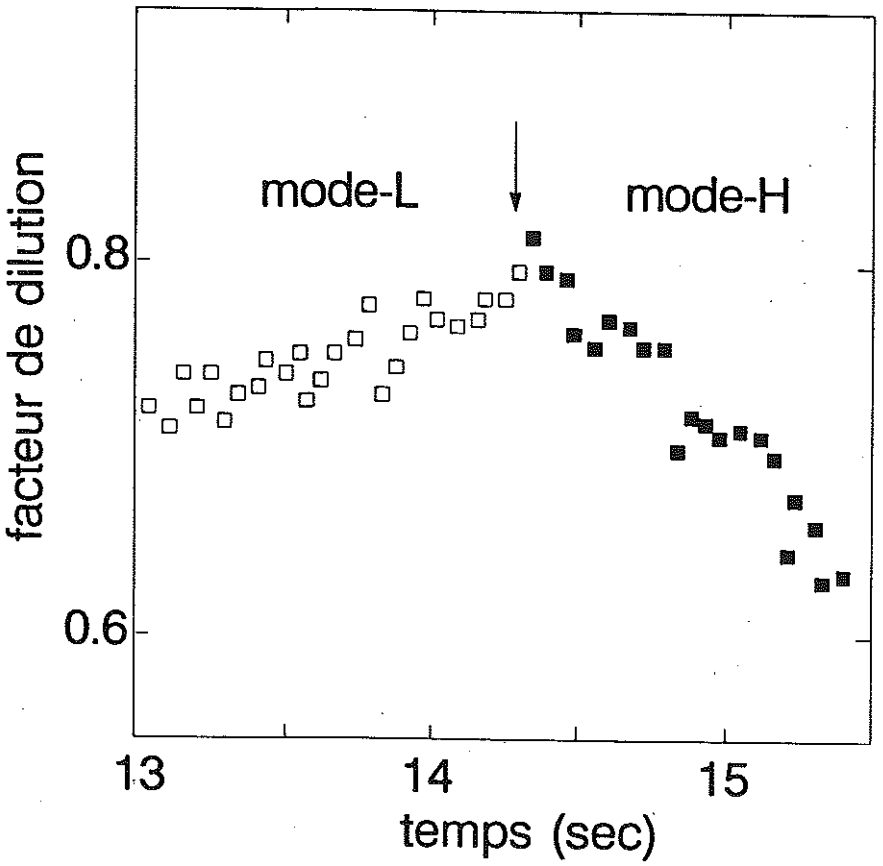

Fig. 5 Evolution of the dilution factor n_D/n_e on axis during discharges a magnetic limiter discharge (JET pulse 10793, $I_p = 3$ MA). The arrow indicates the L to H-mode transition.

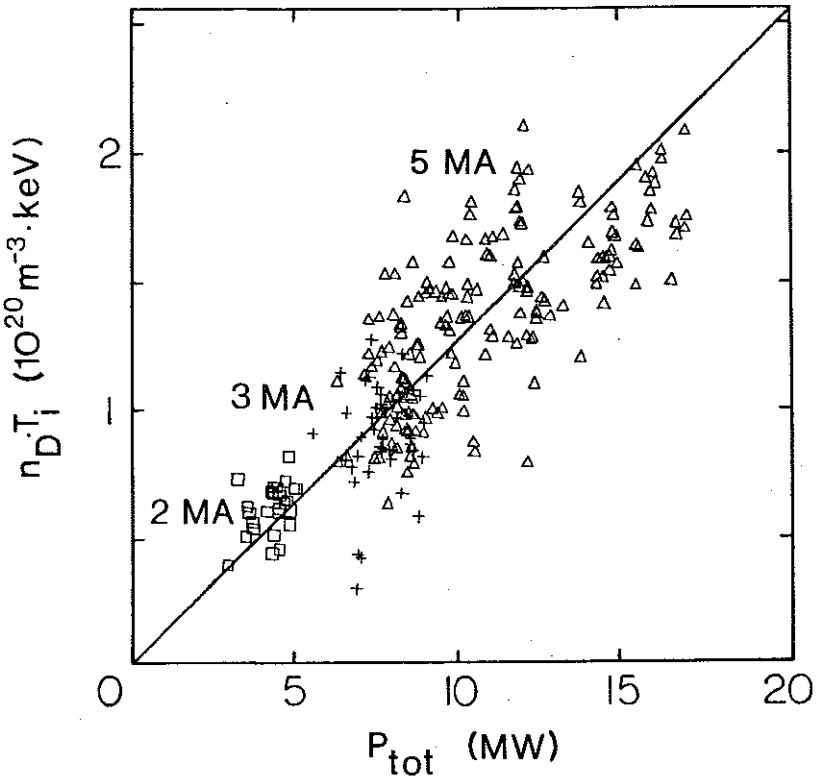

Fig. 6a Variation of the deuterium pressure $n_D T_i$ on axis as a function of the total input power for material limiter discharges.

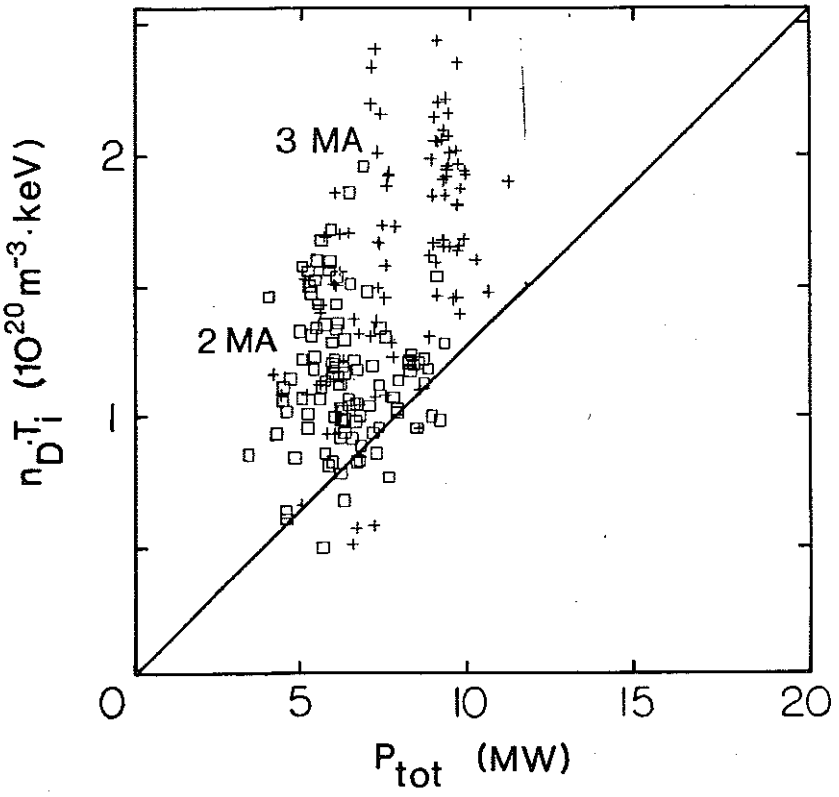

Fig. 6b Variation of the deuterium pressure $n_D T_i$ on axis as a function of the total power during the H-mode phase of magnetic limiter discharges. The line reproduces the dependence observed in Fig. 5a with a material limiter.

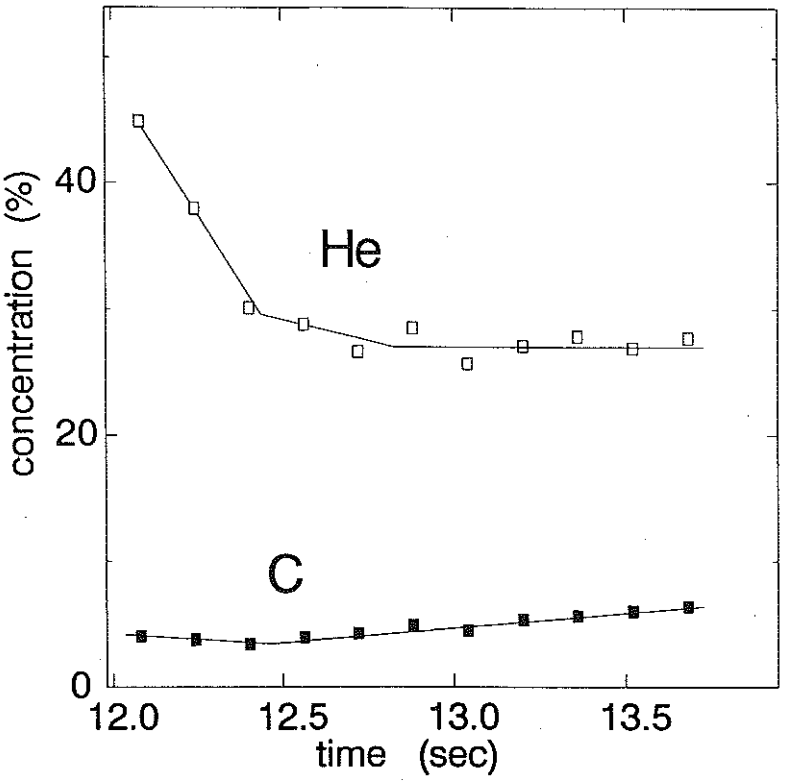

Fig. 7a Evolution of the central carbon and helium concentrations during a helium discharge with a magnetic limiter (JET pulse 10205, $I_p = 3\,\mathrm{MA}$).

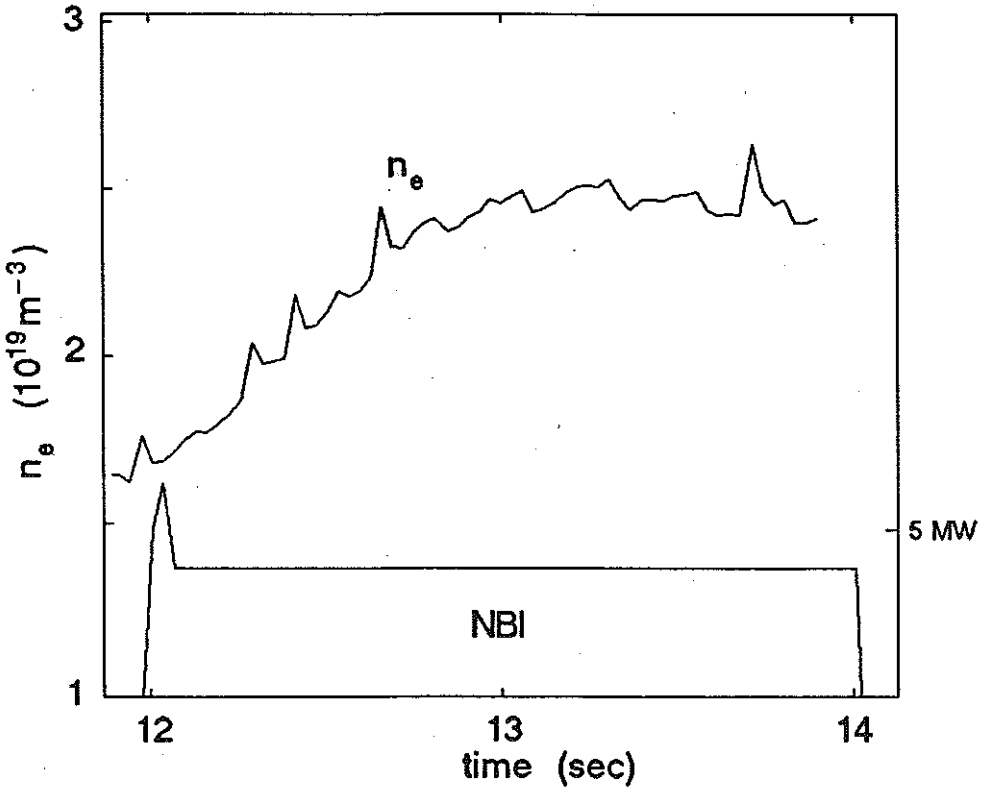

Fig. 7b Evolution of the electron density on axis and the total beam power during pulse 10205.

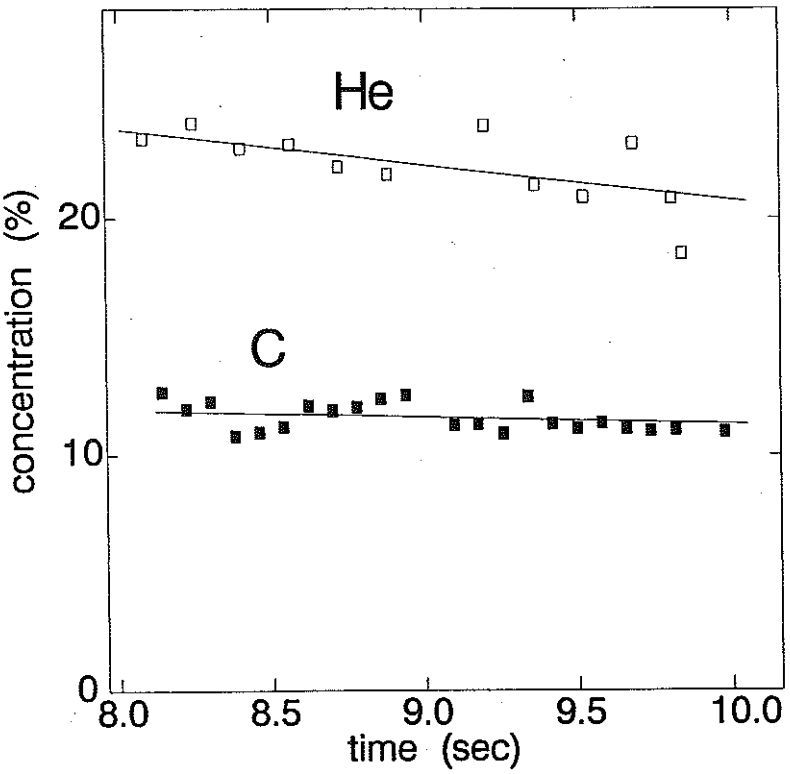

Fig. 8a Evolution of the central carbon and helium concentrations during a helium discharge with a material limiter (JET pulse 10142, $I_p = 3$ MA).

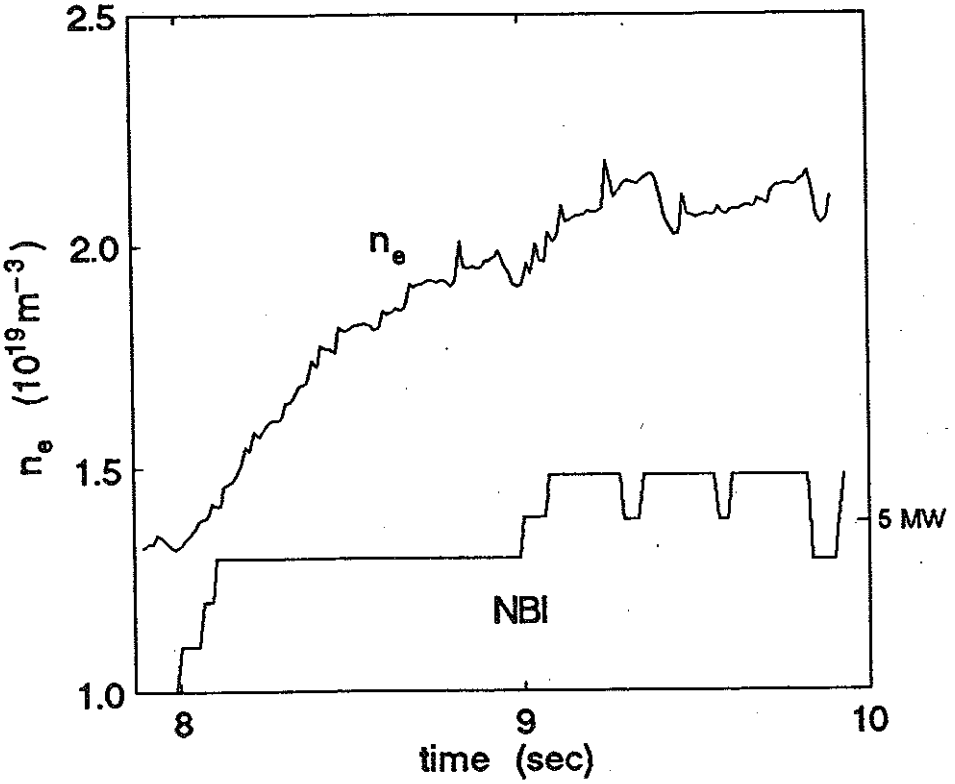

Fig. 8b Evolution of the electron density on axis and the total beam power during pulse 10142.

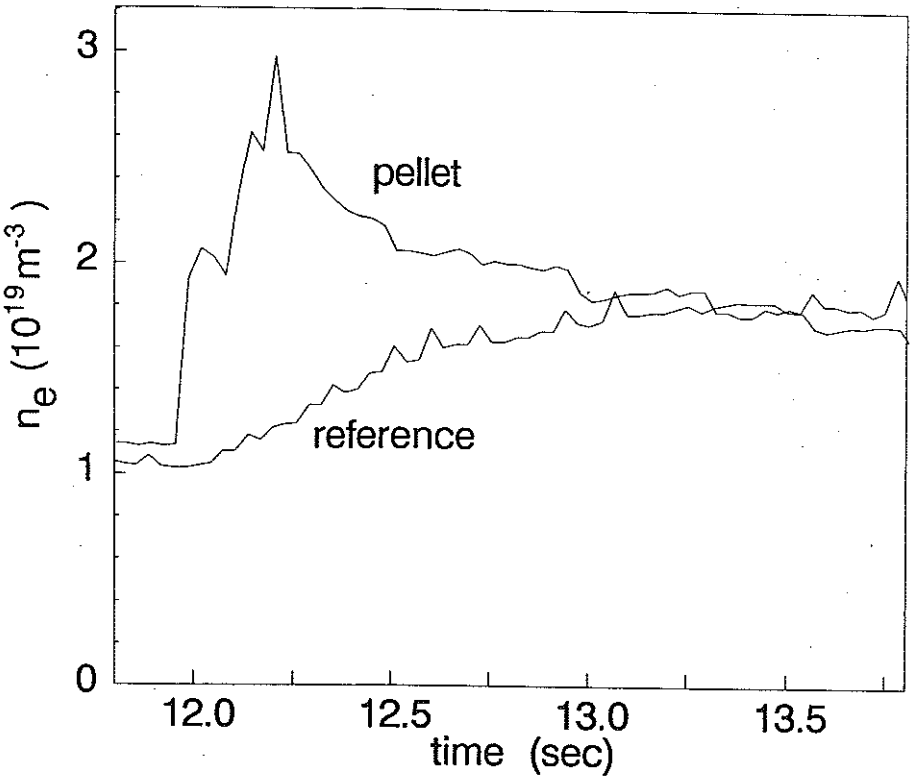

Fig. 9 Variation of the electron density on axis during NB injection starting at 12s with (pellet) and without (reference) injection of a deuterium pellet at 12s.

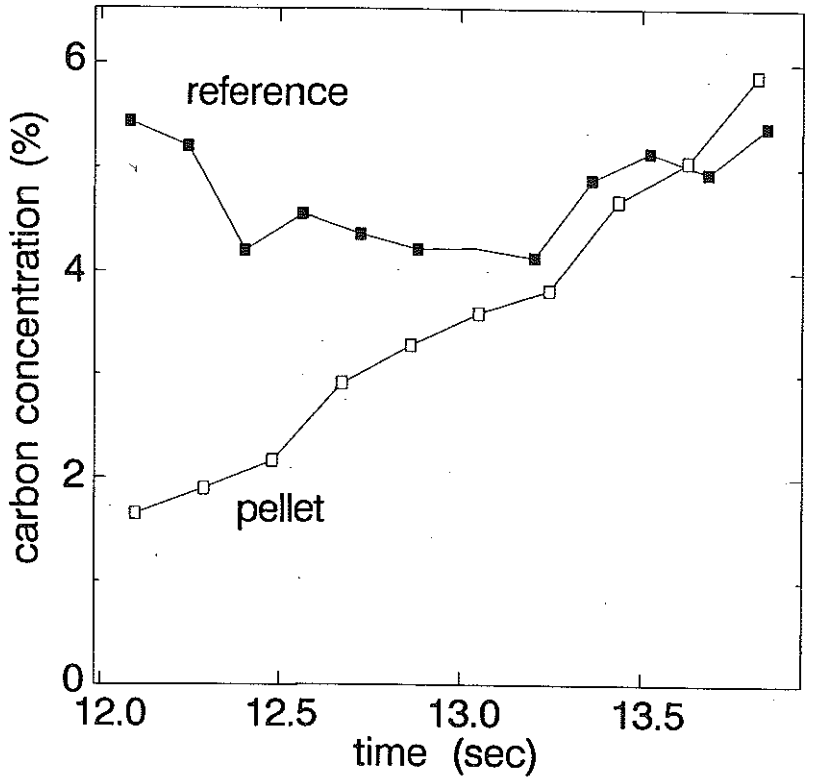

Fig. 10 Evolution of the central carbon concentration with (pellet) and without (reference) pellet injection. At the time indicated by the arrow, the carbon density is approximately 6.0×10^{17} m^{-3} for the pellet case and 6.5×10^{17} m^{-3} for the reference case.

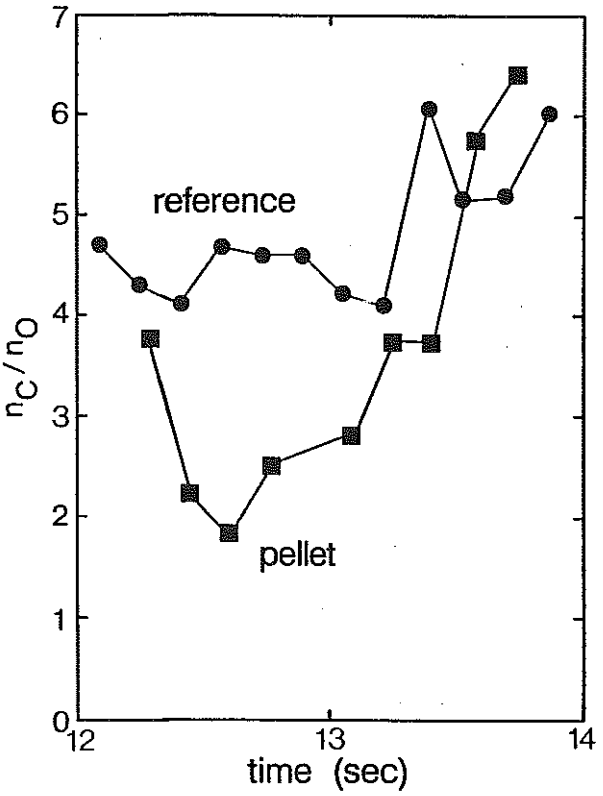

Fig. 11 Evolution of the carbon to oxygen ratio on axis with (pellet) and without (reference) injection of a deuterium pellet.

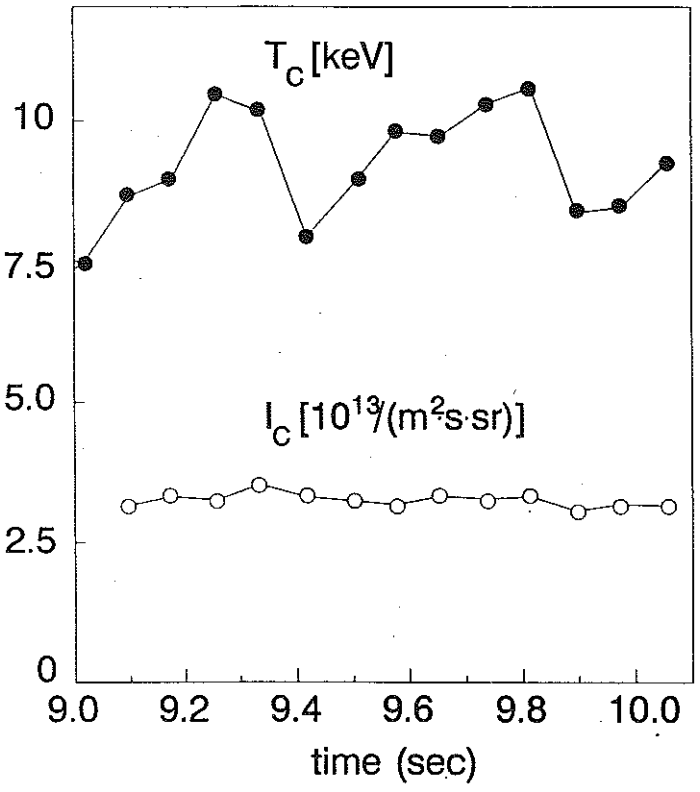

Fig. 12 Evolution of the central ion temperature and line intensity of the carbon n=8-7 transition during sawtooth relaxations.

APPENDIX 1.

THE JET TEAM

JET Joint Undertaking, Abingdon, Oxon, OX14 3EA, U.K.

J.M.Adams[1], F.Alladio[4], H.Altmann, R.J.Anderson, G.Appruzzese, W.Bailey, B.Balet, D.V.Bartlett, L.R.Baylor[24], K.Behringer, A.C.Bell, P.Bertoldi, E.Bertolini, V.Bhatnagar, R.J.Bickerton, A.Boileau[3], T.Bonicelli, S.J.Booth, G.Bosia, M.Botman, D.Boyd[31], H.Brelen, H.Brinkschulte, M.Brusati, T.Budd, M.Bures, T.Businaro[4], H.Buttgereit, D.Cacaut, C.Caldwell-Nichols, D.J.Campbell, P.Card, J.Carwardine, G.Celentano, P.Chabert[27], C.D.Challis, A.Cheetham, J.Christiansen, C.Christodoulopoulos, P.Chuilon, R.Claesen, S.Clement[30], J.P.Coad, P.Colestock[6], S.Conroy[13], M.Cooke, S.Cooper, J.G.Cordey, W.Core, S.Corti, A.E.Costley, G.Cottrell, M.Cox[7], P.Cripwell[13], F.Crisanti[4], D.Cross, H.de Blank[16], J.de Haas[16], L.de Kock, E.Deksnis, G.B.Denne, G.Deschamps, G.Devillars, K.J.Dietz, J.Dobbing, S.E.Dorling, P.G.Doyle, D.F.Düchs, H.Duquenoy, A.Edwards, J.Ehrenberg[14], T.Elevant[12], W.Engelhardt, S.K.Erents[7], L.G.Eriksonn[5], M.Evrard[2], H.Falter, D.Flory, M.Forrest[7], C.Froger, K.Fullard, M.Gadeberg[11], A.Galetsas, R.Galvao[8], A.Gibson, R.D.Gill, A.Gondhalekar, C.Gordon, G.Gorini, C.Gormezano, N.A.Gottardi, C.Gowers, B.J.Green, F.S.Griph, M.Gryzinski[26], R.Haange, G.Hammett[6], W.Han[9], C.J.Hancock, P.J.Harbour, N.C.Hawkes[7], P.Haynes[7], T.Hellsten, J.L.Hemmerich, R.Hemsworth, R.F.Herzog, K.Hirsch[14], J.Hoekzema, W.A.Houlberg[24], J.How, M.Huart, A.Hubbard, T.P.Hughes[32], M.Hugon, M.Huguet, J.Jacquinot, O.N.Jarvis, T.C.Jernigan[24], E.Joffrin, E.M.Jones, L.P.D.F.Jones, T.T.C.Jones, J.Källne, A.Kaye, B.E.Keen, M.Keilhacker, G.J.Kelly, A.Khare[15], S.Knowlton, A.Konstantellos, M.Kovanen[21], P.Kupschus, P.Lallia, J.R.Last, L.Lauro-Taroni, M.Laux[33], K.Lawson[7], E.Lazzaro, M.Lennholm, X.Litaudon, P.Lomas, M.Lorentz-Gottardi[2], C.Lowry, G.Magyar, D.Maisonnier, M.Malacarne, V.Marchese, P.Massmann, L.McCarthy[28], G.McCracken[7], P.Mendonca, P.Meriguet, P.Micozzi[4], S.F.Mills, P.Millward, S.L.Milora[24], A.Moissonnier, P.L.Mondino, D.Moreau[17], P.Morgan, H.Morsi[14], G.Murphy, M.F.Nave, M.Newman, L.Nickesson, P.Nielsen, P.Noll, W.Obert, D.O'Brien, J.O'Rourke, M.G.Pacco-Düchs, M.Pain, S.Papastergiou, D.Pasini[20], M.Paume[27], N.Peacock[7], D.Pearson[13], F.Pegoraro, M.Pick, S.Pitcher[7], J.Plancoulaine, J-P.Poffé, F.Porcelli, R.Prentice, T.Raimondi, J.Ramette[17], J.M.Rax[27], C.Raymond, P-H.Rebut, J.Removille, F.Rimini, D.Robinson[7], A.Rolfe, R.T.Ross, L.Rossi, G.Rupprecht[14], R.Rushton, P.Rutter, H.C.Sack, G.Sadler, N.Salmon[13], H.Salzmann[14], A.Santagiustina, D.Schissel[25], P.H.Schild, M.Schmid, G.Schmidt[6], R.L.Shaw, A.Sibley, R.Simonini, J.Sips[16], P.Smeulders, J.Snipes, S.Sommers, L.Sonnerup, K.Sonnenberg, M.Stamp, P.Stangeby[19], D.Start, C.A.Steed, D.Stork, P.E.Stott, T.E.Stringer, D.Stubberfield, T.Sugie[18], D.Summers, H.Summers[20], J.Taboda-Duarte[22], J.Tagle[30], H.Tamnen, A.Tanga, A.Taroni, C.Tebaldi[23], A.Tesini, P.R.Thomas, E.Thompson, K.Thomsen[11], P.Trevalion, M.Tschudin, B.Tubbing, K.Uchino[29], E.Usselmann, H.van der Beken, M.von Hellermann, T.Wade, C.Walker, B.A.Wallander, M.Walravens, K.Walter, D.Ward, M.L.Watkins, J.Wesson, D.H.Wheeler, J.Wilks, U.Willen[12], D.Wilson, T.Winkel, C.Woodward, M.Wykes, I.D.Young, L.Zannelli, M.Zarnstorff[6], D.Zasche[14], J.W.Zwart.

PERMANENT ADDRESS

1. UKAEA, Harwell, Oxon. UK.
2. EUR-EB Association, LPP-ERM/KMS, B-1040 Brussels, Belgium.
3. Institute National des Récherches Scientifique, Quebec, Canada.
4. ENEA-CENTRO Di Frascati, I-00044 Frascati, Roma, Italy.
5. Chalmers University of Technology, Göteborg, Sweden.
6. Princeton Plasma Physics Laboratory, New Jersey, USA.
7. UKAEA Culham Laboratory, Abingdon, Oxon. UK.
8. Plasma Physics Laboratory, Space Research Institute, Sao José dos Campos, Brazil.
9. Institute of Mathematics, University of Oxford, UK.
10. CRPP/EPFL, 21 Avenue des Bains, CH-1007 Lausanne, Switzerland.
11. Risø National Laboratory, DK-4000 Roskilde, Denmark.
12. Swedish Energy Research Commission, S-10072 Stockholm, Sweden.
13. Imperial College of Science and Technology, University of London, UK.
14. Max Planck Institut für Plasmaphysik, D-8046 Garching bei München, FRG.
15. Institute for Plasma Research, Gandhinagar Bhat Gujat, India.
16. FOM Instituut voor Plasmafysica, 3430 Be Nieuwegein, The Netherlands.
17. Commissiariat à L'Energie Atomique, F-92260 Fontenay-aux-Roses, France.
18. JAERI, Tokai Research Establishment, Tokai-Mura, Naka-Gun, Japan.
19. Institute for Aerospace Studies, University of Toronto, Downsview, Ontario, Canada.
20. University of Strathclyde, Glasgow, G4 ONG, U.K.
21. Nuclear Engineering Laboratory, Lapeenranta University, Finland.
22. JNICT, Lisboa, Portugal.
23. Department of Mathematics, Univeristy of Bologna, Italy.
24. Oak Ridge National Laboratory, Oak Ridge, Tenn., USA.
25. G.A. Technologies, San Diego, California, USA.
26. Institute for Nuclear Studies, Swierk, Poland.
27. Commissiariat à l'Energie Atomique, Cadarache, France.
28. School of Physical Sciences, Flinders University of South Australia, South Australia SO42.
29. Kyushi University, Kasagu Fukuoka, Japan.
30. Centro de Investigaciones Energeticas Medioambientales y Techalogicas, Spain.
31. University of Maryland, College Park, Maryland, USA.
32. University of Essex, Colchester, UK.
33. Akademie de Wissenschaften, Berlin, DDR.

CR 88.49.1A